Materials Today Bio 20 (2023) 100630

Contents lists available at ScienceDirect

Materials Today Bio

journal homepage: www.journals.elsevier.com/materials-today-bio

Incorporation of synthetic water-soluble curcumin polymeric drug within calcium phosphate cements for bone defect repairing

Ying Zhang [a,b,1], Hailiang Xu [a,b,1], Jing Wang [c,1], Xiaochen Fan [d], Fang Tian [a,b], Zhiyuan Wang [a,b], Botao Lu [a,b], Weidong Wu [a,b], Youjun Liu [a,b], Yixiang Ai [a,b], Xiaohui Wang [a,b], Lei Zhu [a,b,***], Shuaijun Jia [a,b,**], Dingjun Hao [a,b,*]

[a] Department of Spine Surgery, Honghui Hospital, Xi'an Jiaotong University, Xi'an, China
[b] Shaanxi Key Laboratory of Spine Bionic Treatment, Xi'an, Shaanxi, China
[c] Science and Technology on Thermostructural Composite Materials Laboratory, Northwestern Polytechnical University, Xi'an, China
[d] Department of Chinese Medicine and Rehabilitation, Honghui Hospital, Xi'an Jiaotong University, Xi'an, China

ARTICLE INFO

Keywords:
Calcium phosphate cement
Curcumin
Hyaluronic acid
Osteogenic activity
Bone defects

ABSTRACT

Modified macroporous structures and active osteogenic substances are necessary to overcome the limited bone regeneration capacity and low degradability of self-curing calcium phosphate cement (CPC). Curcumin (CUR), which possesses strong osteogenic activity and poor aqueous solubility/bioavailability, esterifies the side chains in hyaluronic acid (HA) to form a water-soluble CUR-HA macromolecule. In this study, we incorporated the CUR-HA and glucose microparticles (GMPs) into the CPC powder to fabricate the CUR-HA/GMP/CPC composite, which not only retained the good injectability and mechanical strength of bone cements, but also significantly increased the cement porosity and sustained release property of CUR-HA *in vitro*. CUR-HA incorporation greatly improved the differentiation ability of bone marrow mesenchymal stem cells (BMSCs) to osteoblasts by activating the RUNX family transcription factor 2/fibroblast growth factor 18 (RUNX2/FGF18) signaling pathway, increasing the expression of osteocalcin and enhancing the alkaline phosphatase activity. In addition, *in vivo* implantation of CUR-HA/GMP/CPC into femoral condyle defects dramatically accelerated the degradation rate of cement and boosted local vascularization and osteopontin protein expression, and consequently promoted rapid bone regeneration. Therefore, macroporous CPC based composite cement with CUR-HA shows a remarkable ability to repair bone defects and is a promising translational application of modified CPC in clinical practice.

1. Introduction

Traumatic fractures, osteoporosis, congenital malformations, and tumor resection are the major causes of bone defects [1,2]. Once a bone defect exceeds the critical healing size, it fails to heal independently [3]. Bone grafting is necessary to promote bone regeneration and repair at the defect site, and the effectiveness of bone defect repair is directly related to the clinical outcome [4,5]. Currently used grafting materials and methods for bone defects include autologous, allogeneic, xenograft, and synthetic grafts [6]. Globally, over 2 million bone grafts are transplanted to repair bone defects annually [7]. Autologous bone grafting remains the gold standard for repairing bone defects and is both osteoinductive and osteogenic in nature [8]. However, donor site morbidity and the limited availability of autologous bone have hampered its widespread application in treating bone defects [9].

It is necessary to develop new materials and therapeutic strategies to repair bone defects. Allogeneic bone transplants are associated with an increased risk of immunological rejection, and graft materials are in short

* Corresponding author. Department of Spine Surgery, Honghui Hospital, Xi'an Jiaotong University, Xi'an, China; Shaanxi Key Laboratory of Spine Bionic Treatment, Xi'an, Shaanxi, China.
** Corresponding author. Department of Spine Surgery, Honghui Hospital, Xi'an Jiaotong University, Xi'an, China; Shaanxi Key Laboratory of Spine Bionic Treatment, Xi'an, Shaanxi, China.
*** Corresponding author. Department of Spine Surgery, Honghui Hospital, Xi'an Jiaotong University, Xi'an, China; Shaanxi Key Laboratory of Spine Bionic Treatment, Xi'an, Shaanxi, China.
E-mail addresses: zhulei619@xjtu.edu.cn (L. Zhu), shuaijun9500@hotmail.com (S. Jia), haodingjun@mail.xjtu.edu.cn (D. Hao).
[1] Ying Zhang, Hailiang Xu and Jing Wang contributed equally to this work.

https://doi.org/10.1016/j.mtbio.2023.100630
Received 26 January 2023; Received in revised form 20 March 2023; Accepted 4 April 2023
Available online 7 April 2023

supply and expensive. Over the last few decades, synthetic biomaterials, such as calcium phosphate cement (CPC), polylactic-*co*-glycolic acid (PLGA), and polymethyl methacrylate (PMMA) have been studied for their potential to heal bone defects [10,11]. Therefore, the development and fabrication of new biomimetic osteosynthetic biomaterials is an ideal method for repairing bone defects.

CPC was first described by Brown and Chow in 1985 as a bone replacement materials with high biocompatibility and mineral composition similar to that of the extracellular matrix in real bone. Since then, it has been widely studied in the orthopedic and dental fields [12]. CPC is readily injected and can be shaped to fit the form of the lesion, making it an excellent material for treating complicated bone defects. Although CPC may be used to fill a variety of different forms of bone defects, its lack of porosity after molding, prolonged *in vivo* degradation period, and lack of osteoinductive activity contribute to its limited use in clinical practice [13,14]. First, the intrinsic pore size of CPC is only 1–15 μm after molding, and bone tissue development is restricted to the cement's surface and cannot penetrate into the interior of the cement. Moreover, this naturally formed tiny pore size is not sufficient to support revascularization during bone regeneration [15]. Second, CPC degrades slowly *in vivo*, and its small pore size makes it difficult for bodily fluids to penetrate and flow through it, increasing its degradation time from months to years [16]. These characteristics impede early tissue replacement and filling of bone defects, and interfere with the pathological process of local bone repair. Finally, and most critically, CPC lacks osteoinductive factors, as its main components are inorganic salts, which are not sufficiently biologically active to support the regeneration of bone defects. Therefore, enhancing the osteoinductivity of CPC, optimizing their pore size, and accelerating their degradation rate are necessary to promote widespread clinical application.

Enhancing the osteogenic characteristics of CPCs by the addition of direct or indirect osteodynamic or osteoinductive elements is essential for promoting their clinical translation. Curcumin (CUR), an acidic polyphenol that promotes osteogenic differentiation-promoting properties [17,18]. Xiong et al. showed that CUR enhances the osteogenic development of periodontal ligament stem cells [19]. Sarkar et al. showed that CUR promoted the activity and proliferation of osteoblasts [17]. Curcumin is gradually being used in bone tissue engineering research because of its superior pharmacological activity for osteogenesis *in vitro*. However, the poor water solubility, chemical instability, and poor bioavailability of curcumin in living organisms prevent its osteogenic properties from being maximised *in vivo*. Therefore, we modified curcumin using hyaluronic acid (HA), a natural high molecular weight mucopolysaccharide with good biocompatibility and multiple molecular functional groups. The water solubility of the modified curcumin (CUR-HA) was greatly enhanced, while maintaining its biological activity. In addition, we prepared bionic porous CPCs using 150 μm diameter glucose microparticles (GMP) as porogens. This naturally occurring metabolite can be easily transported intracellularly and solubilized in phosphate-buffered saline after three days to form interconnected macroporous CPCs. The present study was conducted to prepare porous CPCs with easy degradation and osteoinductive properties.

In this study, we fabricated a CUR-HA/CPC composite porous bone replacement cement. We determined the physical properties of the CUR-HA/CPC composite porous bone cement, including the setting time, injectability, porosity, compressive mechanical properties, and morphology, were investigated. Then, an *in vitro* culture model consisting of CUR-HA/CPC composite porous bone cement and bone marrow mesenchymal stem cells (BMSCs) was established, and its biocompatibility, cell proliferation, osteogenic differentiation, and related osteogenic mechanisms were investigated. Finally, the CUR-HA/CPC composite porous bone cement was implanted into the femoral condyle defect site in Sprague–Dawley (SD) rats. Furthermore, micro-computed tomography (micro-CT) and histological staining were used to test its bone-defect healing capacity 4 and 12 weeks after implantation (Fig. 1).

2. Materials and methods

2.1. Synthesis and characterization of CUR-HA compound

HA (360 mg; 0.18 mM; Focus Biotechnology Co. Ltd., China) was dissolved in 10 mL of deionized water in a 100 mL plastic bottle. Then 207 mg (1 mM) of 1-ethyl-(3-dimethylaminopropyl) carbodiimide hydrochloride was added and the mixture was activated for 30 min. Then, 368.4 mg (1.08 mM) of CUR (Solarbio Technology Co.Ltd, China) was dissolved in N,N-dimethylformamide (2.5 mL) for 30 min. Next, the dissolved CUR was added to the prepared HA solution. Then 60 mg of 4-dimethylaminopyridine was added to the solution. and reacted at 37 °C for 8 h. After 6 h, the solution was dialyzed with a molecular weight cutoff of 2500 using a dialysis bag for 24 h. Dialysis water was replaced every 2 h. After dialysis, the reaction mixture was freeze-dried to obtain yellow solid CUR-HA. To verify whether the synthesized CUR-HA formed new chemically covalent bonds, the lyophilized CUR-HA compound powder was analyzed by Fourier transform infrared spectroscopy (FTIR;

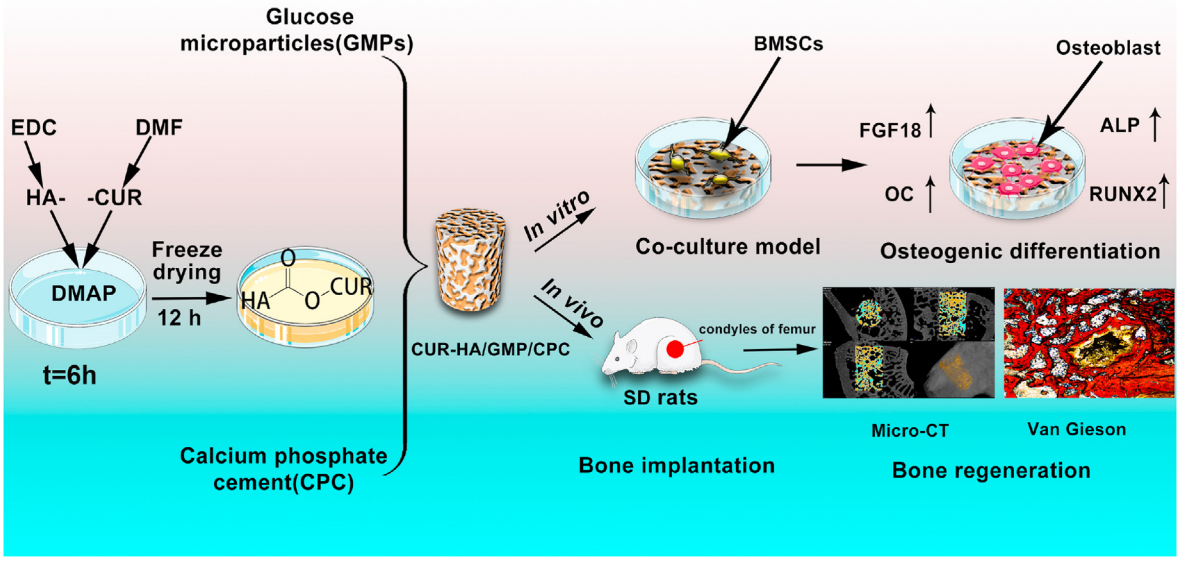

Fig. 1. Schematic diagram for curcumin (CUR)-hyaluronic acid (HA) synthesis and incorporation into calcium phosphate cement (CPC) for bone defect repair.

Perkin-Elmer, CA). FTIR spectroscopy was performed to characterize the chemical bonds in the samples in the range 520–4000 cm^{-1} with a resolution of 2 cm^{-1}. For each FTIR measurement, the sample was scanned 100 times and the spectrum obtained was the average of all scans.

2.2. Measurement of the solubility of CUR-HA and CUR

CUR-HA lyophilized powder (100 mg) and CUR were dissolved in phosphate-buffered saline (PBS buffer, pH 7.4) to saturate and dissolve CUR-HA and CUR respectively, mixed by vortexing for 5 min, and dissolved via ultrasonication for 5 min. The solutions were centrifuged at 14000 rpm/min for 5 min in a high-speed refrigerated centrifuge. The supernatant of the aqueous layer was collected and diluted with dimethyl sulfoxide (DMSO), and the UV absorption values of CUR-HA and CUR solutions were measured at 425 nm by a UV spectrometer. The content and maximum solubility of CUR-HA and CUR were calculated according to the CUR standard curve.

2.3. Preparation of CPC powder

Briefly, 13.2 g of $(NH_4)_2HPO_4$ was dissolved in 250 mL of deionized water and the pH was adjusted to 9 by adding 1 M/L NaOH solution dropwise to obtain 0.1 M/L $(NH_4)_2HPO_4$ solution. Then 28.5 g of $CaCl_2$ was dissolved in 250 mL of deionized water and the pH was adjusted to 9 by adding 1 M/L NaOH solution dropwise to obtain 0.1 M/L $CaCl_2$ solution. The two solutions were then stirred and mixed for 12 h to obtain a low crystallinity hydroxyapatite suspension. Then, 4.8 g of $(NH_4)_2CO_3$ was dissolved in 80 mL of deionized water to obtain 0.05 M/L $(NH_4)_2CO_3$ solution, and 40 mL of 0.1 M/L $CaCl_2$ solution and 80 mL of 0.05 M/L $(NH_4)_2CO_3$ solution were added dropwise to the above suspension to react for 4 h to prepare a hydroxyapatite-coated $CaCO_3$ suspension. After rinsing once, it is dried, ground into a fine powder at 80 °C, calcined at 1500 °C, quick-cooled, grinded for 24 h, and sieved through 500 mesh sieve to prepare the tetracalcium phosphate powder. In addition, the calcium hydrogen phosphate dihydrate was dehydrated at 120 °C for 12 h and anhydrous calcium hydrogen phosphate was added after grinding for 24 h and passing through a 500-mesh sieve. Finally, the produced tetracalcium phosphate, anhydrous calcium hydrogen phosphate and nano-hydroxyapatite were mixed to form the CPC powder. The mass ratio of tetracalcium phosphate to anhydrous calcium hydrogen phosphate was 7:3, and nano-hydroxyapatite accounted for 4% of the total mass of the CPC powder. The percentages of nano hydroxyapatite: tetracalcium phosphate: dicalcium phosphate anhydrous was 4%, 67.24%, 28.84%.

2.4. Preparation of CUR-HA/GMP/CPC composite

A high teflon plastic ring mold (2 mm diameter, 5 mm height) was used to mold the cylindrical CPC bone cement. The 30% of the mold volume was composed of GMP. Then, 8 mg CUR, 8.2 mg HA, or 16.2 mg CUR-HA was added to each set of columns, and the remaining volume was filled with CPC powder. The mixed powder in the cylinder was poured into a new plastic container, and half the volume of the citric acid solution (1% w/w) was added and stirred again for 15 s. The prepared cement was injected into molds (2 mm diameter, 5 mm height), and the samples were left to dry for 24 h at room temperature and 50% relative humidity. Absorbance of CUR (8 mg) was the same as that of 16.2 mg of CUR-HA, which contained the same amount of CUR as detected by spectrophotometer. Moreover, 16.2 mg of CUR-HA contained approximately 8.2 mg of HA, indicating that the CUR molar molecular weights of group CUR/GMP/CPC and group CUR-HA/GMP/CPC are the same. In this way, the materials GMP/CPC, CUR/GMP/CPC, HA/GMP/CPC, and CUR-HA/GMP/CPC were prepared for subsequent analysis.

2.5. Phase composition of CPC

CPC (ground to powder) dried at room temperature for 24 h was used to obtain the X-ray diffraction (XRD) patterns using a SHIMADZU XRD-6100 instrument (Japan). Data was gathered from $2\theta = 10°–80°$ with a step size of 0.02° and a normalized count time of 1.5 s per step. XRD patterns were analyzed by MID jade 6.0. Moreover, the International Centre for Diffraction Data's Joint Committee on Powder Diffraction Standards (JCPDS) reference patterns were used to verify the phase composition.

2.6. CUR-HA release from CUR-HA/CPC composites in vitro

To examine the release characteristics of CUR-HA in CPC, CUR-HA/CPC composite (2 mm diameter, 5 mm high) was immersed in 5 mL of PBS and placed at 37 °C. The UV absorbance values of CUR-HA in PBS were measured 1, 3, 5, 7, 14 and 28 days after immersion using UV spectrophotometer at 425 nm, and the CUR-HA content was calculated based on the CUR standard curve. Time curve of the cumulative release of CUR-HA in CPC was plotted according to the test results.

2.7. Measurement of the setting time of cement

The initial and final setting times of the cements were measured using a Gillmore needle method according to ASTM C266. The groups of CPC cements were prepared into a paste at room temperature and filled into a teflon tubular mold (6 mm diameter, 12 mm height) and quickly moved to the apparatus for measurement. The initial setting time was measured. The test needle was lowered vertically onto the cement surface every 30s and relaxed after 5s, allowing the test rod to be vertically inserted into the cement paste. When the tip of the needle was 4 mm from the bottom plate, the required time was the initial setting time. Immediately after the initial setting time was measured, the test mold with the CPC paste was inverted on the base plate and placed in the stability test chamber. The final setting test pin is used instead of the initial setting test pin. The final setting time of the cements was determined when the test pin did not sink more than l mm into the sample and did not leave a trace on the mold. Six replicate tests were performed and the average value was calculated.

2.8. Injectability examination of cement

Next, we measure the injectability of the CPC. Briefly, groups of cements were filled into a 5 mL syringe fitted with a 1.6 mm inner diameter needle, and a 5 kg compression load was mounted vertically on top of the plunger. The injectivity index was calculated by dividing the mass released from the syringe by the original mass. Injectivity index (%) = (mass of cement paste injected/original mass of cement paste loaded into the syringe) × 100%. Tests were conducted in triplicate. Injectability of the cement paste was determined by the percentage of volume injected. Injectability parameters are related to the experimental conditions.

2.9. Porosity and mechanical testing

Composite cement (2 mm diameter, 5 mm height) was mixed with 20 mL of PBS (pH = 7.4) and incubated at 37 °C on shaker table (100 rpm/min) for three days. PBS buffer was changed every 12 h. After vacuum-drying, the samples were subjected to porosity, mechanical and morphological analysis. Micro-CT was performed using the Skyscan 1172 μCT system, and serial tomograms were reconstructed and analyzed. The porosity was measured in the region of interest (ROI). The compressive strength and elastic modulus of the CPC cylinders (2 mm diameter, 5 mm height) were measured by applying a load of 1 mm/min to the CPC cylinders using a bench machine (INSTRON, USA). Six cylinders were used for each measurement.

2.10. Morphological analysis

Morphology of the CPC composites surface was observed by scanning electron microscopy (SEM, S–3400 N, Japan) before and after leaching.

The surface of each sample was sprayed with gold before scanning.

2.11. In vitro degradation and pH measurements

Prepared bone cement samples ($n = 3$) from each group were immersed in PBS (pH = 7.4) at 37 °C and shaken at a speed of 60 r/min. The ratio of the solution volume to the weight of samples was 20 mL/g. The pH of the solution was measured with a pH meter after 1, 3, 7, 14, 21, and 28 d of incubation, and the PBS solution was changed at each time point. The collected cement samples were rinsed with deionized water and dried at each predetermined intervals. The rate of sample weight loss (WL%) was calculated by the equation: $WL(\%)=(W_0–W_1)/W_0 \times 100\%$. ($W_0$ represents the initial weight of the sample and W_1 represents the dry weight of the sample at each time point.)

2.12. Isolation and culture of primary rat BMSCs

BMSCs were isolated from SD female rats (4 weeks old). SD rats were purchased from the Experimental Animal Center of Xi'an Jiaotong University. All *in vitro* experiments were approved by the Ethics Committee of Honghui Hospital, Xi'an Jiaotong University. First, femurs of rats were cut off with sterile scissors, and the bone marrow cavity was flushed with PBS buffer. The rinsed bone marrow suspension was centrifuged for 5 min at 1200 rpm/min. The centrifuged cells were resuspended in DEME high glucose medium (Gibco, USA) (1% penicillin-streptomycin, 10% fetal bovine serum) and placed in an incubator for culture (37 °C, 5% CO_2). The BMSCs were purified using adherence screening method. Cells were cultured to the 3rd generation for subsequent experiments.

2.13. Cell attachment and proliferation on CPC composites

CPC samples were sterilized in an ethylene oxide sterilizer. BMSCs suspension (1×10^4/mL) were seeded onto each sample in a 24-well plate. After co-culturing for three days, the samples were washed 2 times with PBS and fixed with 4% glutaraldehyde for 4 h. Subsequently, the samples were successively dehydrated with a graded series of ethanol solutions (40%, 60%, 80%, 90%, and 100%), and air-dried at 37 °C overnight. After spraying with gold, the morphology of the cells attached to the CPC samples was observed by scanning electron microscopy (SEM, S–3400 N, Japan). Proliferation assays were performed in 96-well plates (1×10^3 cells/well). BMSCs cultured in DMEM high sugar medium of GMP/CPC complex were used as blank controls for the experiments. Six replicate wells were used for each group. Cell proliferation activity was measured by CCK-8 test at days 1,3,5 and 7 after seeding, and the absorbance value of each group was measured at 450 nm using a spectrophotometer.

2.14. Cytotoxicity assessment

The cytotoxicity of BMSCs was evaluated by calcein AM and propidium iodide (PI) double fluorescence staining. BMSCs were seeded on the surface of CPC and cultured in DMEM high glucose medium (1% penicillin-streptomycin, 10% fetal bovine serum) at a density of 1×10^3 cells. After 7 days of culture, staining was performed according to the instructions of the live-dead viability kit. Cells were observed under a fluorescent microscope. The number of live/dead cells was counted with image J (NIH, USA).

2.15. Osteogenic differentiation

Early osteogenic differentiation of the BMSCs was assessed by alkaline phosphatase (ALP, Solarbio, China) staining and quantification of ALP enzyme activity. Cells were seeded on the CPC surface using the previously described method. After 3 and 7 days of culture, ALP activity was assessed quantitatively and qualitatively using ALP activity assay and staining kit. Late osteogenic differentiation was assessed via Alizarin Red S staining at 14 and 21 d after culture. Samples were fixed with 4% paraformaldehyde for 10 min, stained with 2% Alizarin Red S (ARS, Solarbio, China) for 30 min, and then washed with PBS. The images were captured using anoptical microscope. Quantification of the proportion of ARS-positive regions was performed using Image J (NIH, USA).

2.16. Immunofluorescence staining

BMSCs were fixed with 4% paraformaldehyde after 7 days of growth on the CPC surface. Cells were permeabilized with 0.5% Triton X-100 for 10 min. Samples were washed thrice with PBS for 5 min and incubated with 3% bovine serum albumin solution for 30 min, followed by incubating with primary mouse *anti*-osteopontin (OC, 1:500, Abcam, UK) and rabbit *anti*-RUNX2 (1:500, Affinity, China) antibodies overnight at 4 °C. After washing thrice for 5 min each in PBS, Alexa Fluor 594-labeled donkey anti-mouse and Alexa Fluor 488-labeled donkey anti-rabbit (1:1000, Abcam, UK) were mixed and incubated for 2 h at 37 °C in dark. Samples were then washed with PBS and nuclei were stained with 10 ng/mL DAPI (4′,6-diamidino-2-phenylindole, Beyotime, China). Finally, the samples were imaged by a confocal laser scanning microscope (Zeiss LSM 800, Germany).

2.17. Western blotting analysis and quantitative real-time polymerase chain reaction

Western blotting was performed in according to the descriptions in a previous study [20]. In brief, total protein was separated from cells, and the concentration was detected by the BCA protein assay kit. The protein sample was mixed with an equal volume of 5 × loading buffer followed by boiling at 100 °C for 10min. Protein samples were separated using 8% SDS-PAGE gel electrophoresis and transferred to PVDF membrane. The PVDF membranes were blocked in 5% skimmed milk for 30 min, followed by the addition of primary antibodies for 12 h. Next, the membranes were incubated with a horseradish peroxidase-conjugated secondary antibody. Protein bands were exposed to chemiluminescence reagents and quantified using Image J software. All tests were performed in triplicates. The primary antibodies used for western blotting were RUNX2 (1:1000) and FGF18 (1:1000), β-actin (1:1000) was used as the internal control.

Total RNA was purified from each group of cells using TRizol (Beyotime, China) according to the manufacturer's protocol. After reverse transcription using a reverse transcriptase kit (Beyotime, China), real-time fluorescent quantitative polymerase chain reaction (qPCR) was performed for RUNX2 and FGF18 with SYBR green using a Bio-Rad PCR system (Bio-Rad). β-actin amplication was used as an internal control. The primers used are as follows: RUNX2 Forward: CACTGGAAGTGCAGCAAGA, Reverse: TTACATGACAGCGGTGGCATATC. FGF18 Forward: GAGGAGAACGTGGACTTCCG, Reverse: TCCACTAGGAGCT GGGCATA. β-actin Forward: CTAAGGCCAACCGTGAAAAG, Reverse: TACATGGCTGGGGTGTTGA. Gene expression levels were calculated by the $2^{-\Delta\Delta CT}$ method.

2.18. Surgical procedure

Healthy female SD rats ($n = 24$, 2-month-old) weighing 180–200 g provided by the Experimental Animals Centre of Xi'a Jiaotong University were used as experimental animals. The protocol was approved by the Animal Ethics Committee of Honghui Hospital, Xi'a Jiaotong University and was in accordance with the institutional guidelines for the care and use of laboratory animals. All rats were divided into four groups: (1) GMP/CPC, (2) CUR/GMP/CPC, (3) HA/GMP/CPC, and (4) CUR-HA/GMP/CPC. All rats were anesthetized by intraperitoneal (IP) injection of 1% pentobarbital (60 mg/kg). The hind limbs of the rats were shaved and sterilized with iodophor disinfectant. A longitudinal incision was made through the lateral femoral distal joint. The femoral distal condyle was exposed, with a width of 2 mm and a depth of 5 mm hole was drilled,

which was washed twice with sterile saline. Cement paste was injected into the condylar defects ($n = 6$ in each group), and the subcutaneous tissue and skin were sequentially sutured. Postoperative antibiotics (cefazolin, 15 mg/kg) were routinely administered to prevent infection. The general conditions of the animals, including feeding, activity, and wound healing, were observed postoperatively. After 4 and 12 weeks of implantation, the rats were euthanized using an overdose of pentobarbital, and the femoral condyles were harvested for evaluation.

2.19. Micro-CT scanning

The femoral condyles were collected and excess soft tissue was removed. The samples were fixed in 4% paraformaldehyde (PFA) at 4 °C for 24 h, then scanned by micro-CT (Y.XLON, Germany). To determine the degradation of cement and new bone formation, trabecular bone structure software trabecular bone volume fraction (BV/TV) and trabecular number (Tb) analyses were performed using Geminy software. Parametric analysis was performed on newly formed bone using segmentation thresholds of 158–221 and on whole bone using thresholds of 158–1000 (bone cement is more dense than newly formed trabeculae and residual bone cement is brighter than trabeculae on Micro CT images). The implantation region of each cement was chosen as the region of interest (ROI).

2.20. Histological analysis

Each femoral condyle was fixed in 4% paraformaldehyde for 2 days and dehydrated in a graded series of ethanol. Femoral condyle was embedded with methyl methacrylate, followed by 30 μm continuous sectioning using a Leica 1600 hard tissue sectioning machine. Sections were stained with haematoxylin-eosin, Van Gieson stain, and immunohistochemical staining (OPN, 1:300) were examined under a light microscope (Leica, Germany). Images of 5 different slices were randomly from the VG images for analysis. The trabecular number and separation were measured.

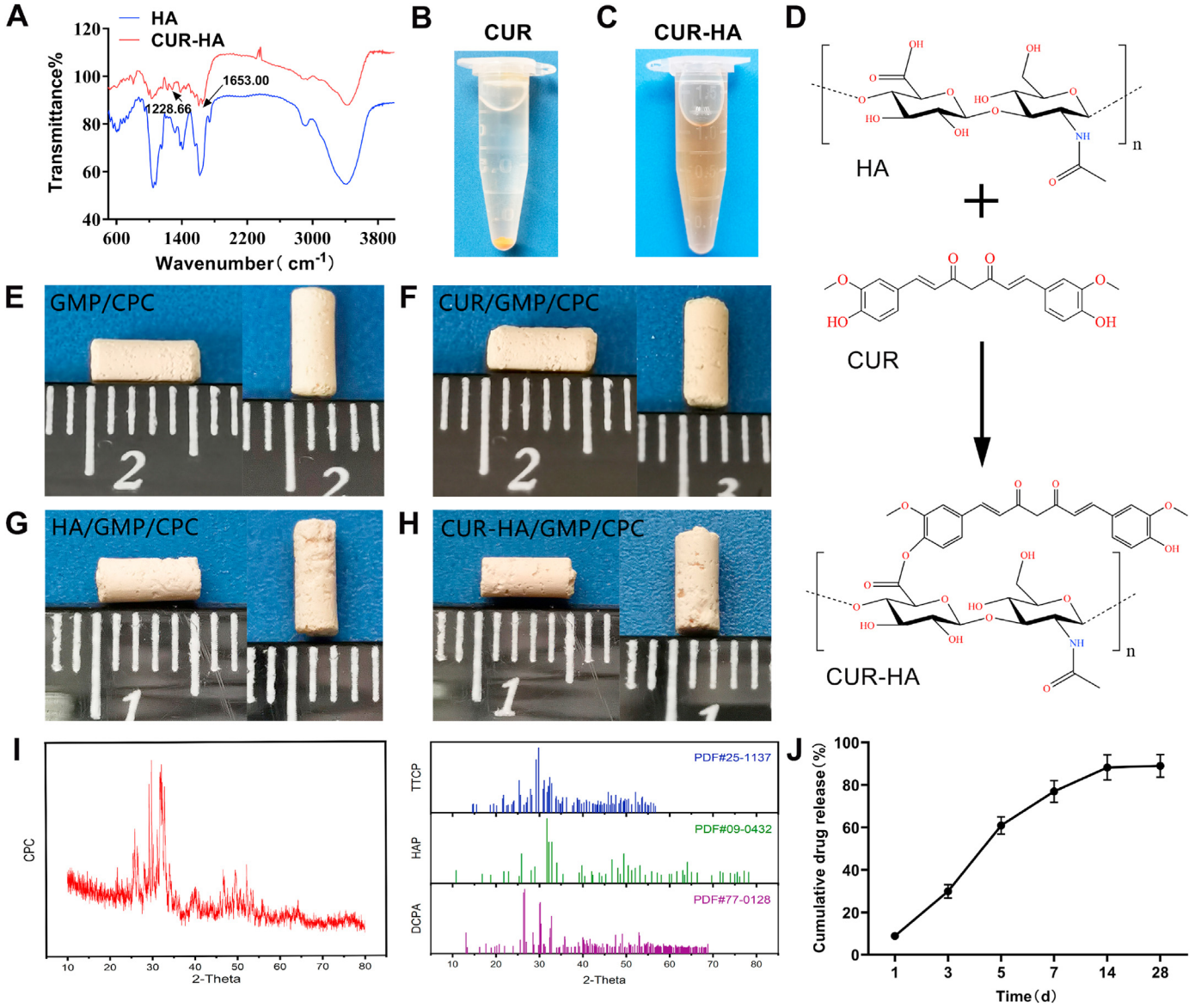

Fig. 2. Characterization of CUR-HA and preparation of composite CPC cement. (A) Infrared spectrum of CUR-HA polymeric drug. (B) CUR is insoluble in water. (C) CUR-HA is water-soluble. (D) Synthetic equation of CUR-HA. (E–H) Glucose microparticle (GMP)/CPC, CUR/GMP/CPC, HA/GMP/CPC and CUR-HA/GMP/CPC samples. (I) Phase composition of CPC. (J) *In vitro* release profile of CUR-HA in CUR-HA/GMP/CPC.

2.21. Statistical analysis

Data were processed using SPSS version 19 software. The data were expressed as the mean ± standard deviation. Multiple groups comparisons were performed by ANOVA, and two means were compared by the least significant difference method. Differences were considered statistically significant at $p < 0.05$.

3. Results

3.1. Characterization of CUR-HA and its release pattern from CPC composite in vitro

The CUR-HA was characterized using a Fourier transform infrared spectrometer (FTIR). Compared to HA, the absorption peak at 1510.26 cm^{-1} in the FTIR spectra of the CUR-HA was related to the C=C vibration of the benzene ring, and the peak at 3421.72 cm^{-1} was attributed to the –OH group in the CUR structure. The absorption peaks at 1228.66 and 1653.00 cm^{-1} are characteristic of an ester (R–CO–OR) functional group (Fig. 2A). This result indicated successful conjugation between CUR and HA. CUR was completely insoluble in water, and powder precipitation was visible at the bottom of the water (Fig. 2B and C). In contrast, CUR-HA exhibited good solubility in water. HA and CUR undergo a condensation reaction to generate CUR-HA, as shown in Fig. 2D.

General appearances of the CPC composites in the four group are shown in Fig. 2E–H. The phase composition of CPC was examined by XRD. The main product in CPC was hydroxyapatite (HAP), and incomplete initial components tetracalcium phosphate (TTCP) and dicalcium phosphate anhydrous (DCPA) were also present (Fig. 2I). To characterize the release of CUR-HA from the CPC composite, we soaked the CUR-HA/GMP/CPC composite in PBS *in vitro* and calculated the amount of CUR components released in the solution by measuring the absorbance value of the soaking solution at 425 nm by UV spectrophotometer. As shown in Fig. 2J, CUR-HA was gradually released from the CPC over time, with a faster release early on, reaching a cumulative release of 89% of the total content by 28 d.

3.2. Characterizations of the setting time, injectability, porosity and mechanical parameters of the cements

As shown in Fig. 3A, the initial setting time of (5.6 ± 0.8) min and the final setting time of (15.3 ± 0.9) min in the CUR-HA/GMP/CPC group were higher than those of the remaining three groups. There were no significant differences in the initial and final setting times among the remaining three groups.

The cement paste was tested before coagulation to evaluate its injectivity index of the cement. The injection index of the CUR-HA/GMP/CPC group was (91.3 ± 2.3)%, and the difference was not statistically significant compared to all other groups, GMP/CPC (92.2 ± 1.0)%; CUR/GMP/CPC (85.5 ± 4.3)%; HA/GMP/CPC (91.1 ± 1.7)%. This also indicates that neither CUR-HA or GMP affected the injectability of CPC.

The three-dimensional structure of the bone cement was measured and analyzed using micro-CT. The incorporation of GMP was effective in porogenizing the CPC (Fig. 3B). The introduction of GMPs led to the formation of large pores during the cement setting. As the GMPs dissolved, the porosities of the cements in different groups ranged from 40% to 45%. The porosity of the cement in each group did not differ significantly.

The compressive strengths and elastic modulus of the cement samples before and after leaching are presented in Fig. 3C and D. The compressive strength and elastic modulus decreased after CUR-HA/GMP/CPC group samples were leached for three days, compressive strength changed from (16.60 ± 1.80) to (13.41 ± 1.62) Mpa ($P > 0.05$), and elastic modulus from (0.59 ± 0.51) to (0.46 ± 0.65) Gpa ($P > 0.05$). There were no statistically significant differences in the mechanical parameters of the four groups before or after leaching, indicating that the incorporation of CUR-HA did not affect the mechanical properties of the CPC.

3.3. Surface morphology and pore size distribution of CPCs

Morphologies of the cement samples before and after soaking in PBS for 1 h are shown in Fig. 3E. As shown in Fig. 3E, the cement surfaces of the CUR/GMP/CPC and CUR-HA/GMP/CPC groups were smoother than those of the GMP/CPC and HA/GMP/CPC groups before soaking in PBS. Macroporous structures were not observed on the cements surface in each group. When the samples were dissolved in PBS for 1 h, a smooth macroporous structure appeared. In addition, the pore diameter in each group of cement ranges from 150 to 200 μm, and the pores are uniformly distributed.

3.4. In vitro degradation and pH detection

To evaluate whether the four groups of composite bone cement materials produced acid during degradation, we incubated the samples of the four groups under physiological conditions for 4 weeks. The pH values of the four groups showed a decreasing trend (Fig. 3F). However, the pH values of all groups stabilized from days 1 to day 14 and were in the range of 6.5–7.2. Overall, the pH values of the materials in all the groups never fell below 6, indicating that no acidic material was produced during the degradation of the samples.

All four CPC groups gradually degraded *in vitro*. Weight loss in the CUR-HA/GMP/CPC group was greater than that in the other groups after day 3 (Fig. 3G). At day 28, the weight loss in the CUR-HA/GMP/CPC group was as high as 25.1%, whereas that in the GMP/CPC group was only 10.4% ($P < 0.05$).

3.5. Adhesion and proliferation of BMSCs on CPCs in vitro

BMSCs grew and adhered well to the surface of the cement in all groups in a long shuttle shape (Fig. 4A–D). The SEM images show that the cell density was significantly higher in the CUR-HA/GMP/CPC group compared to the other groups, although the initial cell seeding density was the same among the groups. This indicated that CUR-HA/GMP/CPC significantly promoted the proliferation and adhesion of BMSCs.

As depicted in Fig. 4E, cell proliferation was analyzed by CCK-8 kit at four time points. Proliferation of BMSCs in all groups over time. However, the proliferation rate of BMSCs in the CUR-HA/GMP/CPC group was significantly higher than that in the other three groups after 3, 5, 7 d of culture. We also found that the rate of live cells in the CUR-HA/GMP/CPC group was 97% while the rate of dead cells was 3%, which was not statistically significance compared to the other groups (Fig. 4F–J). This also indicated that CUR or CUR-HA did not induce the death of BMSCs.

3.6. Alizarin red S staining and ALP activity

As the BMSCs gradually grew on the CPC composites, the orange-red complexes were deposited more intensively. All four groups had mineralized calcium nodules on day 14, which also indicated the osteogenic induction activity of the cements in each group ($P > 0.05$). However, after 21 d of culture, the CUR-HA/GMP/CPC group had denser mineralized nodules, which were significantly better than those of the other three groups ($P < 0.05$) (Fig. 5A and D).

Staining and analysis of ALP activity after BMSCs were seeded on the surface of each group of CPC composites are shown in Fig. 5B, D. Three days after seeding, there was no statistical difference in the activity of ALP among the groups ($P > 0.05$). In contrast, on day 7 after BMSC seeding, ALP activity in the CUR-HA/GMP/CPC group was significantly higher than that in the other groups ($P < 0.05$).

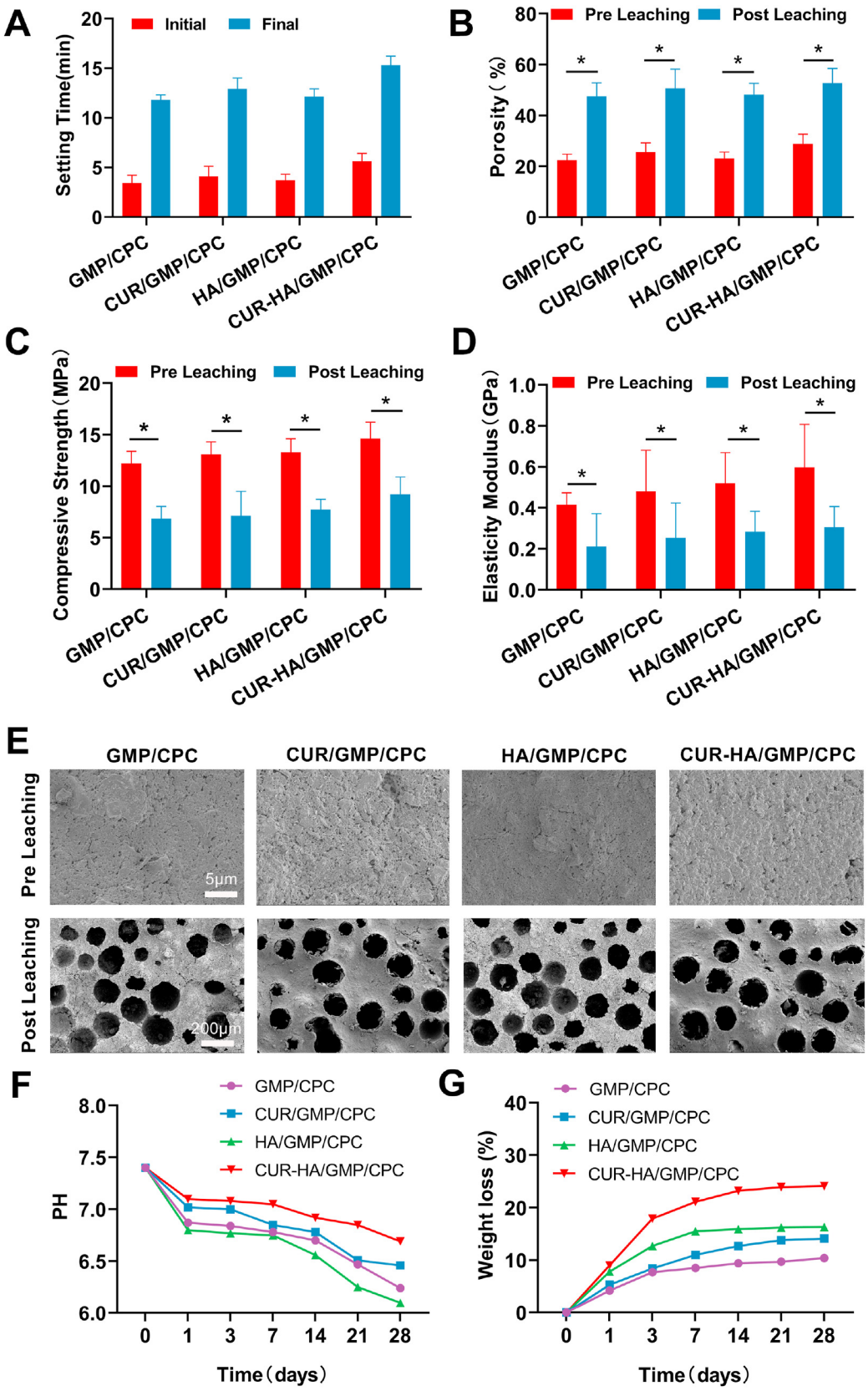

Fig. 3. Physicochemical properties, mechanical strength and scanning electron microscopy (SEM) observations of different bone cements. (A) Comparison of the initial and final setting time among groups. (B) Porosity of the composite cement was evaluated before and after leaching in PBS for 1 h. (C) Compressive strength and (D) elastic modulus of cements were evaluated before and after leaching for 1 h. (E) Surface morphology of cements was observed using SEM before (pre-leaching) and after 1 h of leaching into PBS at 37 °C (post-leaching). (F) PH of the cement-soaked PBS at different time points. (G) Weight loss rates of cements at different time points. ($n = 3$, $^*P < 0.05$).

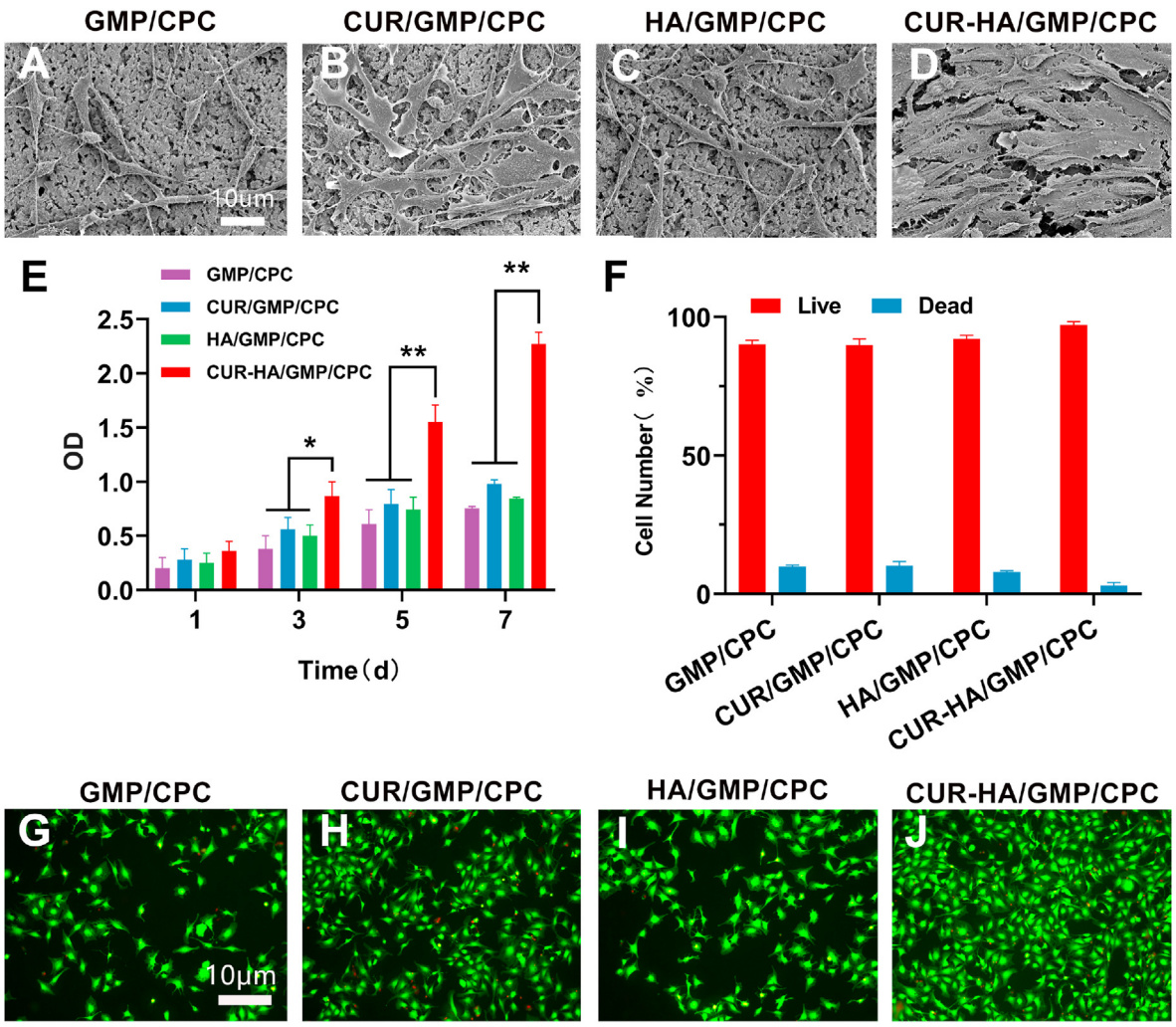

Fig. 4. Growth morphology, proliferation and activity of BMSCs in CPC. (A–D) BMSCs seeded on the surface of cements and observed via SEM after 3 days culture. (E) CCK-8 assay detects the proliferation of BMSCs on cements from days 1–7. (F) Live/Dead cell count of BMSCs on different cement on the 7th day. (G–J) Staining image of dead and live BMSCs growing on CPC surfaces of four groups on the 7th days. Green indicates live cells, and red color means dead cells. ($n = 3$, $^*P < 0.05$). (For interpretation of the references to color in this figure legend, the reader is referred to the Web version of this article.)

3.7. Evaluation of osteogenic differentiation by immunofluorescence and western blotting

To further explore the osteogenic differentiation of BMSCs on the surface of each CPC group and the activity of differentiated osteoblasts, RUNX2 and OC double-label immunofluorescence staining was performed (Fig. 6A). An osteoblast-like morphology was observed in all four groups of cells, and all OC markers were positive. However, the OC-positive cells were more densely distributed in the CUR-HA/GMP/CPC group. The RUNX2 fluorescence intensity and range of cells in the CUR-HA/GMP/CPC group were higher than those in the other groups, indicating that CUR-HA/GMP/CPC can effectively promote the differentiation of BMSCs into osteoblasts and maintain the osteoblast phenotype.

RUNX2 plays an essential role in the osteoblast differentiation of BMSCs, and FGF18 is a crucial protein for osteogenic differentiation. To evaluate the osteogenic differentiation effects of the CUR-treated cement, we analyzed the expression level of RUNX2 and FGF18 in BMSCs cultureed on CPC composites for 7 days (Fig. 6B–D). We found that the mRNA expression of RUNX2 and FGF18 in CUR-HA/GMP/CPC group was up-regulated, and its protein expression was increased significantly compared to other three groups ($P < 0.05$). In addition, the quantitative analysis showed no significant differences among the GMP/CPC, CUR/GMP/CPC and HA/GMP/CPC groups (Fig. 6E and F). These results further suggest that the CUR-HA composite cement has an excellent osteogenic differentiation effect.

3.8. Micro-CT reconstruction and quantification

Micro-CT was used to scan and reconstruct 3D images of the repaired bone defects in rats at 4 (Fig. 7A) and 12 weeks (Fig. 7B) after bone cement implantation. The degree of bone defect repair, cement degradation and new bone formation were evaluated by micro-CT 3D images.

At 4 weeks, 58.7% of the cyan-labeled bone cement was visible in the CUR-HA/GMP/CPC group, which was significantly lower than that in the other three groups ($P < 0.05$; no statistical difference between the remaining 3 groups.) (Fig. 7C). At week 12, the percentage of yellow-labeled new cancellous bone visible in the CUR-HA/GMP/CPC group was 60.8%, which was significantly higher than that in the other three groups ($P < 0.05$; no statistical difference between the remaining 3 groups.) (Fig. 7D). This value was 37.2% in the CUR/GMP/CPC group. In addition, the percentage of new cancellous bone visible in the GMP/CPC group was 29% at 12 weeks, which was the lowest among all four groups ($P < 0.05$). Using horizontal, sagittal and coronal 3D image

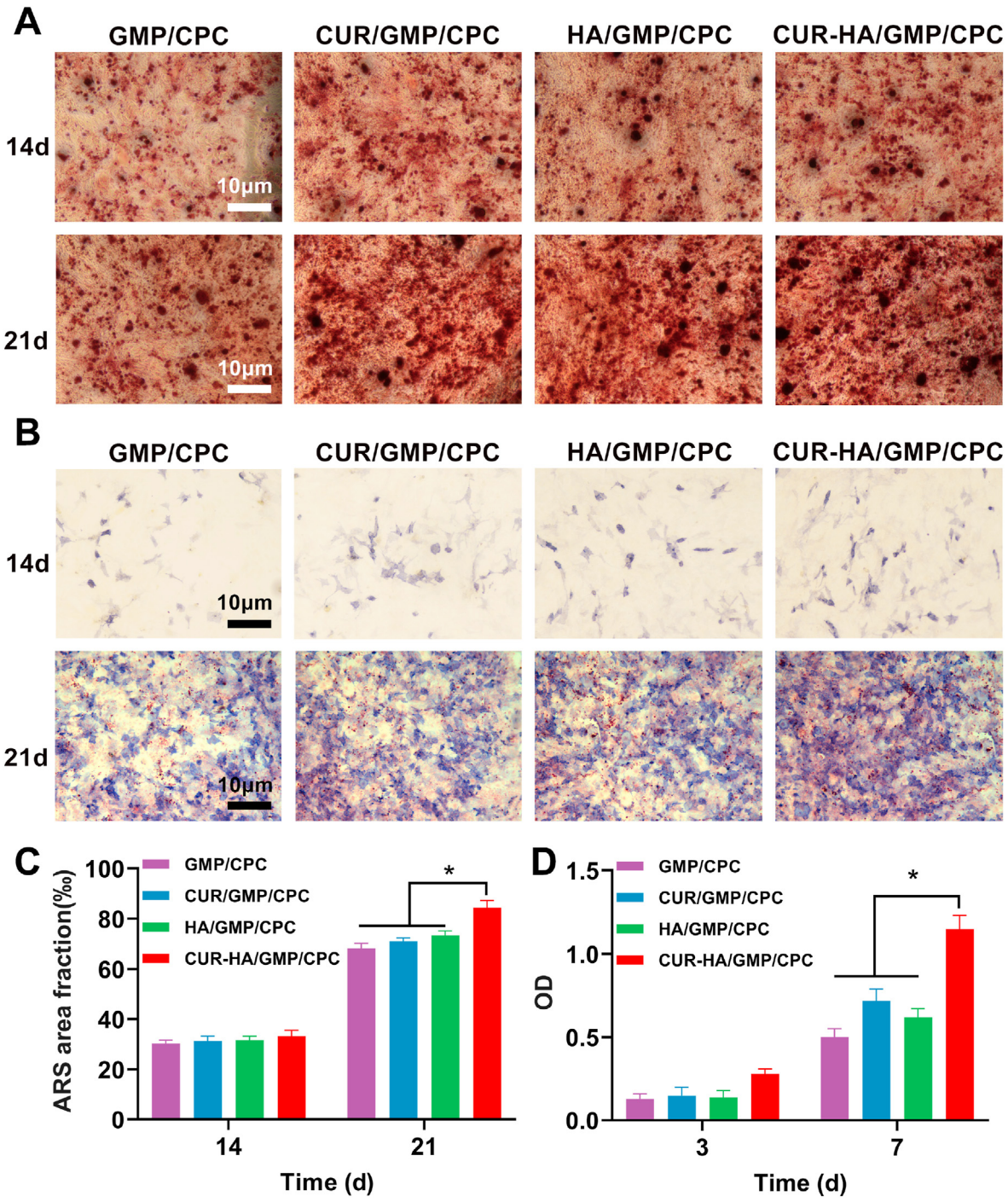

Fig. 5. Alizarin Red S staining and ALP activity. (A) Mineralized nodules are stained with alizarin red S on days 14 and 21 after BMSCs seeded on CPC cement surface. The minerals are dark red. (B) Alkaline phosphatase (ALP) staining of BMSCs after growing on CPC for 3 days or 7 days. The blue represents ALP, and red represents nuclei. (C) Quantification of the proportion of ARS-positive regions on days 14 and 21. (D) Quantification of ALP activity on days 3 and 7. Scale bar = 10 μm. ($n = 3$, $^*P < 0.05$). (For interpretation of the references to color in this figure legend, the reader is referred to the Web version of this article.)

reconstructions, we found that the cancellous bone network formed in the CUR-HA/GMP/CPC group at 12 weeks was very close to the normal cancellous bone structure.

3.9. Histological analysis

Histological images taken four weeks after implantation are shown in Fig. 8A1–D1. A little bone cement degradation was observed in the GMP/CPC group. The boundary between the bone defect and the bone cement was clearly visible in the GMP/CPC group, and no trabecular-like structures were observed at the edges of the defect. This indicated that there was almost no new bone formation inside the bone cement (Fig. 8A1). CUR/GMP/CPC and HA/GMP/CPC groups showed signs of cement degradation at the periphery of the cement, with some of the degraded areas replaced by new trabeculae (Fig. 8B1–C1). However, the CUR-HA/GMP/CPC group showed significant bone cement degradation, and new bone formation, with new bone trabeculae filling the middle and edges of the bone cement (Fig. 8D1).

At 12 weeks, bone-cement degradation and new bone formation were not significantly improved in the GMP/CPC group (Fig. 8A2). The cement

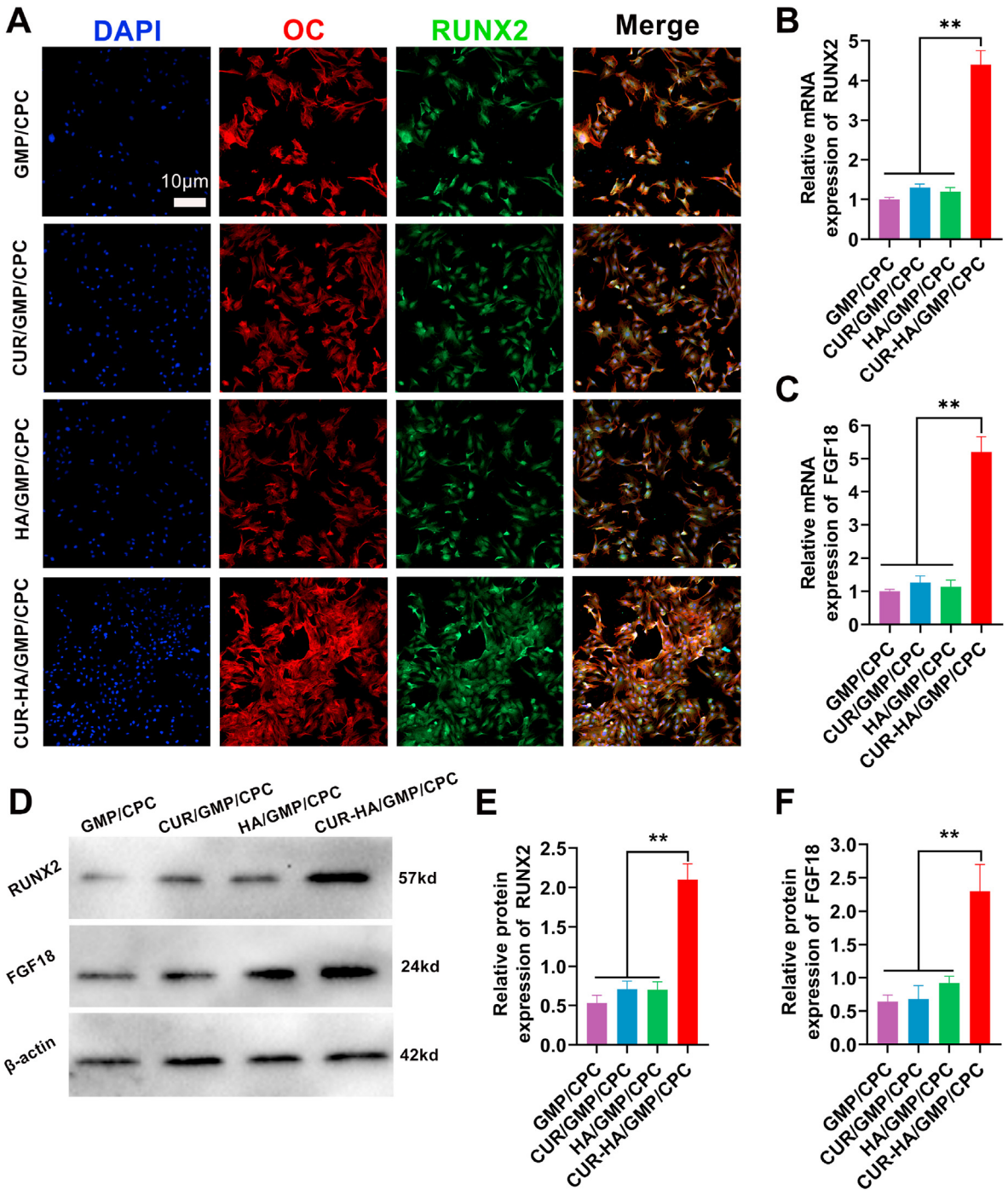

Fig. 6. Identification of osteogenic differentiation of BMSCs by immunofluorescence, western blotting and qRT-PCR. (A) Immunofluorescent staining of OC and RUNX2 in BMSCs seeded onto the cements. Blue color represents nuclei, red represents OC, and the green represents RUNX2. The qRT-PCR assay of osteogenic differentiation of BMSCs cultured for 7 days: (B) RUNX2, (C) FGF18. (D) Protein Strip of RUNX2 and FGF18 in BMSCs growing on cements for 7 days by western blotting assays. The β-actin served as an internal reference gene (E, F) Quantitative analysis of RUNX2 and FGF18 expression levels. ($n = 3$, $^{**}P < 0.01$). (For interpretation of the references to color in this figure legend, the reader is referred to the Web version of this article.)

in the CUR/GMP/CPC group was moderately degraded, and new bone formation was found in the area of cement degradation (Fig. 8B2). The HA/GMP/CPC group showed that new bone formation occurred mainly in the outer region of the bone cement (Fig. 8C2). The CUR-HA/GMP/CPC group showed that the cement was greater degraded and lost its structural integrity, and high magnification images showed that the new cancellous bone had formed a reticular structure at the border of the degraded cement (Fig. 8D2). The inner area of the implanted cement was filled with a large amount of cancellous bone. These results indicate that CUR-HA/GMP/CPC showed excellent degradation and osteogenic activity.

The lateral images of the femoral condyle surgery area are shown in Fig. 8A3-D4. Quantitative histological analysis showed that the trabecular number was significantly higher in the CUR-HA/GMP/CPC group than in the other groups four weeks after surgery (Fig. 8E). The trabecular separation in the CUR-HA/GMP/CPC group was higher than that of other groups at 12 weeks (Fig. 8F). Importantly, immune staining study (Fig. 9) demonstrated that the CUR-HA/GMP/CPC group had a uniform

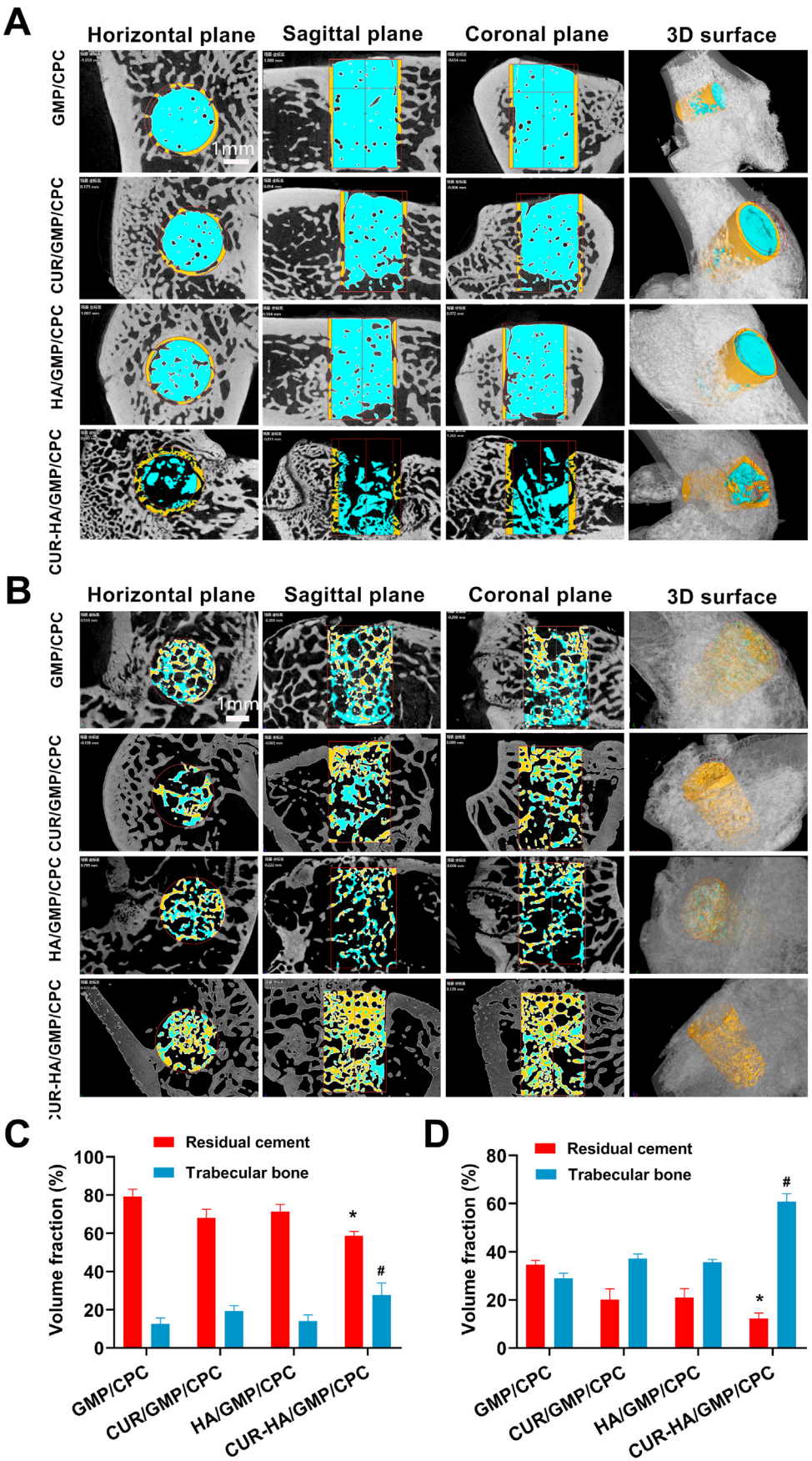

Fig. 7. Micro-CT analysis of cement. (A) 3-dimensional reconstruction of the defect area after 4 weeks implantation. (B) 3-dimensional reconstruction of the defect area after 12 weeks implantation. The yellow part represents newly formed bone, and the green part represents residual cement. (C) Quantitative analysis of residual cement and trabecular bone volume at 4 weeks after implantation. (D) Quantitative analysis of residual cement and trabecular bone volume at 12 weeks after implantation. ($n = 6$, *, #$P < 0.01$). (For interpretation of the references to color in this figure legend, the reader is referred to the Web version of this article.)

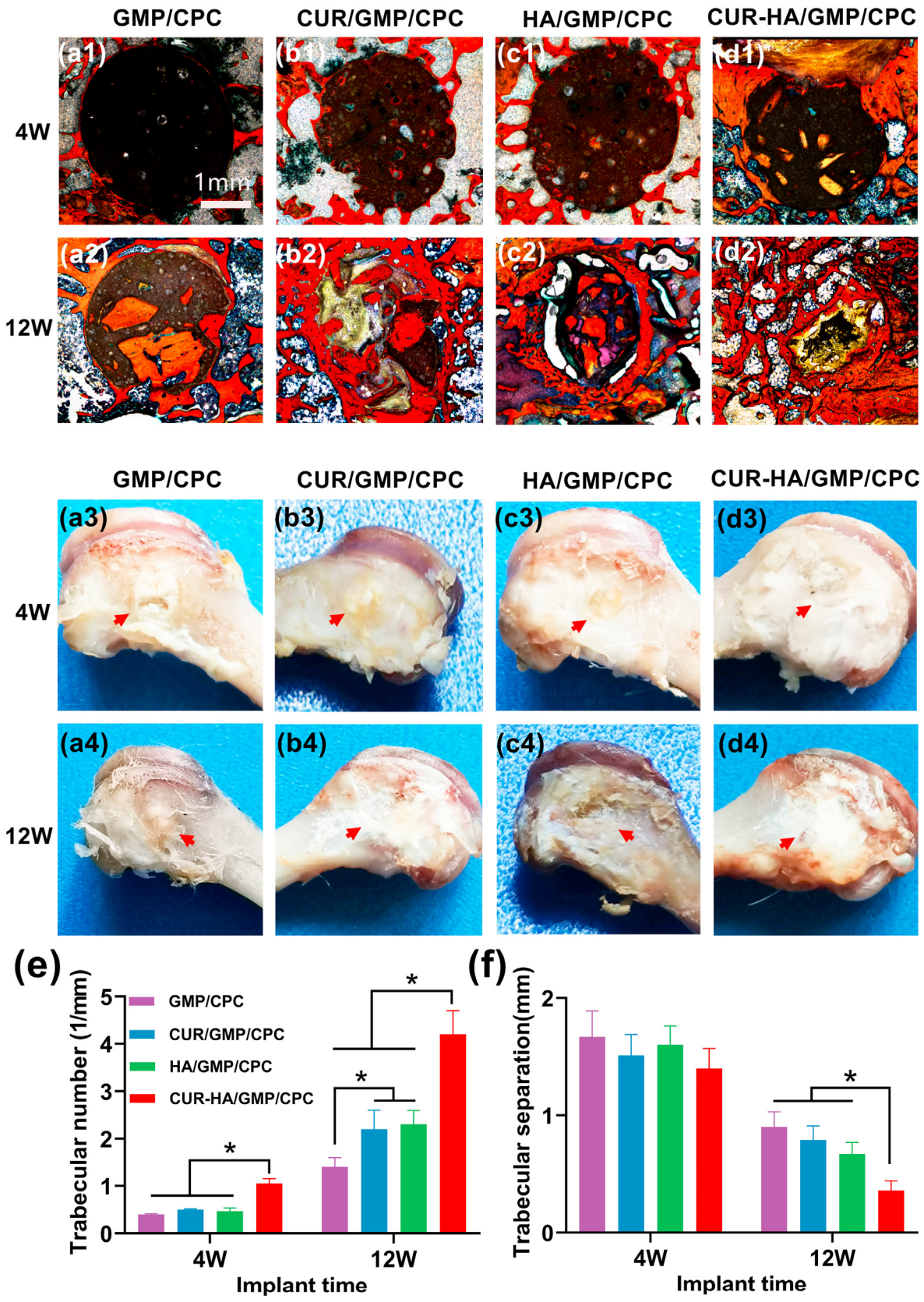

Fig. 8. Histological analysis via Van Gieson staining to assess osteogenesis 4 and 12 weeks after cement implantation. The post-operative femoral condyle images are shown in the lower panel of figure. (A) GMP/CPC, (B) CUR/GMP/CPC, (C) HA/GMP/CPC, (D) CUR-HA/GMP/CPC. (E–F) Quantitative analysis of new bone formation (trabecular number and separation) levels within implantation region at 4 and 12 weeks after surgery. Scale bar = 1 mm. ($n = 6$, $^*P < 0.05$).

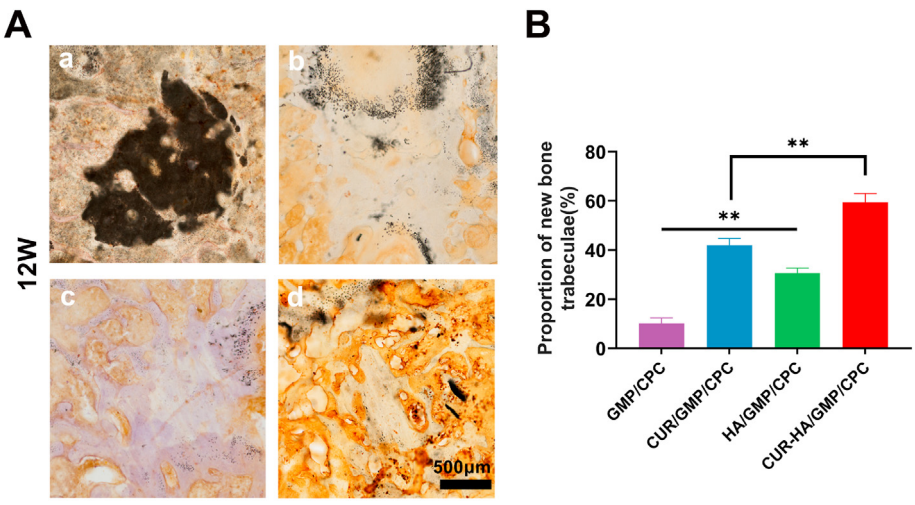

Fig. 9. Immunostaining of osteopontin (OPN) 12 weeks after implantation. (A) a) GMP/CPC, b) CUR/GMP/CPC, c) HA/GMP/CPC, and d) CUR-HA/GMP/CPC. (B) Quantification of the proportion of newly formed bone trabeculae by OPN immunostaining. Scale bar = 500 mm ($n = 6$, $^{**}P < 0.01$).

distribution of trabecular structures in the cement implantation area and strong positive staining for OPN. The GMP/CPC group showed that the bone cement remained undegraded and weak OPN expression presented in the surrounding area. The CUR/GMP/CPC and HA/GMP/CPC groups showed a small amount of trabecular growth in the graft area, and weakly positive OPN expression was observed in the new bone trabeculae.

4. Discussion

CPC has been widely studied for bone defect repair because of its injectability, mechanical properties, and biocompatibility [21,22]. However, CPC has low osteogenic activity, and the absence of porosity after setting is detrimental to new bone ingrowth. Enhancing the osteogenic activity and porosity of CPC after setting is critical to promote its therapeutic applicability. In this study, we esterified CUR, a compound with high osteogenic activity but low solubility, with HA to create novel CUR-HA macromolecule with excellent solubility. In addition, we added 150 μm diameter glucose microspheres to the CPC to create the bionic pore of the bone cement, resulting in a CUR-HA/GMP/CPC composite bone cement. CUR-HA was constantly released from CUR-HA/GMP/CPC composites in PBS for at least 28 d. Furthermore, CUR-HA/GMP/CPC was found to accelerate the degradation of calcium phosphate and other inorganic compositions of cement in rat femoral condyle defects, enhanced the local osteogenic activity, and improve the formation of new bone, resulting in the formation of an effective cancellous bone mesh structure and a suitable repair of the bone defect.

Given potential medical value of CPC, its modification for improved application in bone defect repair has been a popular research topic in recent years [23,24]. Growth factors and active proteins including platelet-rich plasma, bovine collagen, BMP-2, and gelatin, have been added to the CPC [25–28]. Trace elements with osteogenic activity, such as Sr, Mg, Co, Zn, and Si, have also been added to CPC [29–31]. All these active substances can improve the osteogenic activity of CPC to a certain level. However, biologically active ingredients are always potentially immunogenic and their introduction into CPC makes the disinfection process cumbersome and raises the cost of CPC. The safety range of many inorganic ions is narrow, and uncontrolled release of inorganic ions can even cause malignant events such as poisoning. In contrast, natural materials with low immunogenicity and a wide range of sources are more suitable for CPC modification. But natural plant-derived substances, such as CUR are less typically employed to modify CPCs. This may be due to the fact that the isolated active chemicals from plants have limited osteogenic activity or low water solubility. CUR is an excellent antioxidant and also has anticancer properties [32,33]. Meanwhile, Chen et al. found that curcumin has significant anti-inflammatory effects by inhibiting IL-1β and TNF-α release, and promotes tendon-bone interface healing through local curcumin release [18]. In recent research, CUR has also been shown to have a robust osteogenic differentiation effect on stem cells and increase osteoblastic activity [34,35]. Curcumin treatment reduced the expression of matrix metalloproteinase (MMP)-1 but upregulated the expression of the immunomodulatory gene indoleamine 2, 3-dioxygenase (IDO) 1, which in turn inhibited lipogenic differentiation and enhanced osteogenic differentiation of BMSCs [36]. However, these compounds exhibit low water solubility and limited bioavailability. There are few studies on the modification of CUR, and enhancing its water solubility and bioavailability is the key to promoting its clinical application [37,38]. For this reason, we introduced hyaluronic acid (HA) as a material for CUR modification. Hyaluronic acid is a mucopolysaccharide that is widely distributed in the body and functions as a skeletal material in the intercellular matrix, with good water solubility and non-immunogenicity. The molecular backbone of hyaluronic acid contains changeable groups that may be combined directly with a range of medicines to generate molecular carriers for the production of drug delivery systems [39–41]. Therefore, we generated CUR-HA macromolecules by esterifying HA with CUR. Additionally, FTIR analysis revealed that CUR-HA formed ester bonds, and its water solubility was significantly increased. The early release pattern of CUR-HA was consistent with the pathological developmental cycle of bone defect repair. Previous studies on the biological properties of CUR often required its dissolution in organic solvents, such as DMSO, which are highly biotoxic, limiting the amount of CUR used in *vitro* and *in vivo* studies, and indirectly diminishing its biological effects [42]. In the present study, we found that the CUR-HA/GMP/CPC composite significantly enhanced the proliferation and osteogenic differentiation of BMSCs *in vitro*, as well as their osteogenic potential. To further study the mechanism by which CUR-HA promoted BMSC differentiation into osteoblasts, we observed that RUNX2 and FGF18 proteins were considerably highly expressed in the CUR-HA/GMP/CPC group. FGF18 has been shown in several studies to promote osteogenic differentiation, cellular osteogenic activity, and bone tissue regeneration [43]. This finding unequivocally demonstrates that synthesized CUR-HA conserved the biological activity of CUR and did not diminish it due to the esterification step. It has been investigated that the slow release of CUR promotes the opening of glucose transporter 1 in BMSCs, which in turn activates RUNX2 to promote their osteogenic differentiation.This has also led to a deeper understanding of the complex molecular mechanism of CUR in osteogenesis of BMSCs [44].

In addition to the incorporation of bioactive chemicals into CPC to increase its osteogenic activity *in vivo*, morphological changes in CPC

during molding are also critical for increasing its bioactivity [11]. Previous studies also confirmed that unmodified solid CPC degrades little in the early stages [45,46]. This does not fit effectively into the fracture healing pathological cycle, and only provides mechanical stabilization of the fractured bone. Moreover, a mismatch between the degradation of the CPC and the new bone can lead to a delayed healing or non-healing of the fracture. The three-dimensional pore structure facilitates cell adhesion, migration, growth, nutrition and metabolite transfer. The most suitable pore size for osteoblast migration and proliferation is between 40 and 150 m. PLGA particles are combined with CPC and injected *in vivo* to achieve pore formation while also promoting the early development of new bone into the bone defect [47]. Real et al. used a CO_2 bubble-forming reaction between NaH_2PO_4 and $NaHCO_3$ to manufacture CPCs with a porosity of up to 50% [48]. It is worth considering that the use of foaming agents to formulate holes may not be suitable for *in vivo* applications due to the potential risk of gas embolism in patients. Furthermore, it is frequently more difficult to manage the density and width of the pores formed by this gas. As a porogenic agent, we employed glucose particles with high water solubility, which may produce homogeneous pores early in the bone cement formation process. The porosity of the fabricated bone cement was in the range of 40–45%, which is compatible with the standards for cancellous bone. Use of carboxymethylcellulose as a water-soluble porogenic agent also resulted in good CPC porosity. The period of hematoma organization after fracture is the main period of migration of osteoblasts, mesenchymal cells, and other cells to the defect area, and unformed porosity in the early bone cement affects the migration of cells and hinders new bone formation [49]. We used glucose particles, which are rapidly water soluble, as porogenic agents. The glucose particles do not affect the pH value of the curing solution, and the diameter of the glucose particles can be artificially selected to produce CPC porous scaffolds with different pore sizes. Additionally, we found that the mechanical characteristics of the 40% porosity CUR-HA/GMP/CPC composite were reduced, which is consistent with previous research that increased the porosity of CPC.

After implantation of CPC, hydroxyapatite produced during the curing process and some of its own inorganic components are gradually degraded and deposited by proteins such as the extracellular matrix. As the microporous surface gradually transitions from an inorganic interface to a biological interface, the process of stimulating bone formation *in vivo* is facilitated by this transition. There was a considerable rise in the amount of new bone in the CUR-HA/GMP/CPC group, as well as a significant decrease in the volume of residual cement, when CUR-HA was incorporated into the bone cement. The histological HE stained images showed more new bone growth surrounding the CUR-HA/GMP/CPC implants, which is consistent with the data from *in vitro* cell culture. CUR can stimulate endothelial cell migration, thereby increasing vascularization [50]. Bone neogenesis benefits from the development of new blood vessels. Migration of blood vessels is necessary for bone formation. The new blood vessels provide oxygen and nutrients to the bone, while transporting metabolic products and CO_2 accumulated by the cells. Therefore, it is reasonable to speculate that this neovascularization may also be a factor involved in promoting CPC degradation, local cellular metabolism levels and translocation of cellular metabolites and CPC degradation products. Due to the phase change that occurs after bone cement implantation, biomechanical testing of the resected specimens was not performed to determine the bone-implant stability. Determining the stability of the bone-implant interface is an important issue for future research.

5. Conclusions

In this study, CUR was successfully esterified with HA to synthesize a water-soluble CUR-HA macromolecule. Incorporation of CUR-HA did not significantly degrade the injectability and mechanical parameters of CPC. *In vitro* experiments confirmed that the CUR-HA/GMP/CPC composite promoted the differentiation of BMSCs into osteoblasts through the RUNX2/FGF18 signaling pathway. *In vivo* experiments revealed that the incorporation of CUR-HA accelerated the degradation of CPC and promoted new bone formation. Therefore, the water-soluble CUR-HA macromolecule developed in this study can exert osteogenic effects *in vivo*, which is expected to promote the clinical application of active CPCs.

Credit author statement

Ying Zhang: Conceptualization, Methodology, Writing–original draft. **Hailiang Xu**: Conceptualization, Methodology, Writing –original draft. **Jing Wang**: Methodology, Formal analysis. **Xiaochen Fan**: Investigation. **Fang Tian**: Visualization, Data curation. Zhiyuan Wang: Visualization, Investigation, Data curation. **Botao Lu**: Visualization. Weidong Wu: Formal analysis. **Youjun Liu**: Formal analysis, Investigation. **Yixiang Ai**: Visualization, Investigation. **Xiaohui Wang**: Visualization, Investigation. **Lei Zhu**: Conceptualization, Methodology, Supervision. **Shuaijun Jia**: Conceptualization, Methodology, Supervision, Funding acquisition. **Dingjun Hao**: Conceptualization, Methodology, Supervision, Funding acquisition.

Declaration of competing interest

The authors declare that they have no known competing financial interests or personal relationships that could have appeared to influence the work reported in this paper.

Data availability

Data will be made available on request.

Acknowledgments

This work was supported by the key project of the National Natural Science Foundation of China (81830077); Natural Science Foundation of Shaanxi Province (2022SF-005), China. Xi'an Science and Technology Plan Project (2018xasj1004), China.

References

[1] P.H. Warnke, I.N. Springer, J. Wiltfang, Y. Acil, H. Eufinger, M. Wehmoller, H. Terheyden, Growth and transplantation of a custom vascularised bone graft in a man, Lancet 364 (2004) 766–770, https://doi.org/10.1016/S0140-6736(04)16935-3.

[2] Z.J. Balogh, M.K. Reumann, R.L. Gruen, P. Mayer-Kuckuk, M.A. Schuetz, I.A. Harris, M. Bhandari, Advances and future directions for management of trauma patients with musculoskeletal injuries, Lancet 380 (2012) 1109–1119, https://doi.org/10.1016/S0140-6736(12)60991-X.

[3] X. Wu, T. Zhang, B. Hoff, S. Suvarnapathaki, D. Lantigua, C. McCarthy, G. Camci-Unal, Mineralized hydrogels induce bone regeneration in critical size cranial defects, Adv. Healthc. Mater. 10 (2021), e2001101, https://doi.org/10.1002/adhm.202001101.

[4] D. Li, Z. Yang, Y. Luo, X. Zhao, M. Tian, P. Kang, Delivery of MiR335-5p-pendant tetrahedron DNA nanostructures using an injectable heparin lithium hydrogel for challenging bone defects in steroid-associated osteonecrosis, Adv. Healthc. Mater. 11 (2022), e2101412, https://doi.org/10.1002/adhm.202101412.

[5] J. Lee, S. Lee, S.J. Huh, B.J. Kang, H. Shin, Directed regeneration of osteochondral tissue by hierarchical assembly of spatially organized composite spheroids, Adv. Sci. 9 (2022), e2103525, https://doi.org/10.1002/advs.202103525.

[6] B. Dalisson, B. Charbonnier, A. Aoude, M. Gilardino, E. Harvey, N. Makhoul, J. Barralet, Skeletal regeneration for segmental bone loss: vascularised grafts, analogues and surrogates, Acta Biomater. 136 (2021) 37–55, https://doi.org/10.1016/j.actbio.2021.09.053.

[7] V. Campana, G. Milano, E. Pagano, M. Barba, C. Cicione, G. Salonna, G. Logroscino, Bone substitutes in orthopaedic surgery: from basic science to clinical practice, J. Mater. Sci. Mater. Med. 25 (2014) 2445–2461, https://doi.org/10.1007/s10856-014-5240-2.

[8] Z. Bao, Z. Gu, J. Xu, M. Zhao, G. Liu, J. Wu, Acid-responsive composite hydrogel platform with space-controllable stiffness and calcium supply for enhanced bone regeneration, Chem. Eng. J. 396 (2020), 125353, https://doi.org/10.1016/j.cej.2020.125353.

[9] Y.-Q. Tang, Q.-Y. Wang, Q.-F. Ke, C.-Q. Zhang, J.-J. Guan, Y.-P. Guo, Mineralization of ytterbium-doped hydroxyapatite nanorod arrays in magnetic chitosan scaffolds improves osteogenic and angiogenic abilities for bone defect healing, Chem. Eng. J. 387 (2020), 124166, https://doi.org/10.1016/j.cej.2020.124166.

[10] Y. Lai, Y. Li, H. Cao, J. Long, X. Wang, L. Li, L. Qin, Osteogenic magnesium incorporated into PLGA/TCP porous scaffold by 3D printing for repairing challenging bone defect, Biomaterials 197 (2019) 207–219, https://doi.org/10.1016/j.biomaterials.2019.01.013.
[11] A.R. Armiento, L.P. Hatt, G. Sanchez Rosenberg, K. Thompson, M.J. Stoddart, Functional biomaterials for bone regeneration: a lesson in complex biology, Adv. Funct. Mater. 30 (2020), 1909874, https://doi.org/10.1002/adfm.201909874.
[12] Y. Lin, S. Huang, R. Zou, X. Gao, J. Ruan, M.D. Weir, H.H.K. Xu, Calcium phosphate cement scaffold with stem cell co-culture and prevascularization for dental and craniofacial bone tissue engineering, Dent. Mater. 35 (2019) 1031–1041, https://doi.org/10.1016/j.dental.2019.04.009.
[13] I. Lodoso-Torrecilla, N.A.P. van Gestel, L. Diaz-Gomez, E.C. Grosfeld, K. Laperre, J.G.C. Wolke, J. van den Beucken, Multimodal pore formation in calcium phosphate cements, J. Biomed. Mater. Res. 106 (2018) 500–509, https://doi.org/10.1002/jbm.a.36245.
[14] Y. Xia, Y. Guo, Z. Yang, H. Chen, K. Ren, M.D. Weir, H.H.K. Xu, Iron oxide nanoparticle-calcium phosphate cement enhanced the osteogenic activities of stem cells through WNT/beta-catenin signaling, Mater. Sci. Eng. C Mater. Biol. Appl. 104 (2019), 109955, https://doi.org/10.1016/j.msec.2019.109955.
[15] M.A. Lopez-Heredia, K. Sariibrahimoglu, W. Yang, M. Bohner, D. Yamashita, A. Kunstar, J.A. Jansen, Influence of the pore generator on the evolution of the mechanical properties and the porosity and interconnectivity of a calcium phosphate cement, Acta Biomater. 8 (2012) 404–414, https://doi.org/10.1016/j.actbio.2011.08.010.
[16] B. Yang, Y. Zuo, Q. Zou, L. Li, J. Li, Y. Man, Y. Li, Effect of ultrafine poly(epsilon-caprolactone) fibers on calcium phosphate cement: in vitro degradation and in vivo regeneration, Int. J. Nanomed. 11 (2016) 163–177, https://doi.org/10.2147/IJN.S91596.
[17] N. Sarkar, S. Bose, Liposome-encapsulated curcumin-loaded 3D printed scaffold for bone tissue engineering, ACS Appl. Mater. Interfaces 11 (2019) 17184–17192, https://doi.org/10.1021/acsami.9b01218.
[18] B. Chen, Y. Liang, J. Zhang, L. Bai, M. Xu, Q. Han, Z. Yin, Synergistic enhancement of tendon-to-bone healing via anti-inflammatory and pro-differentiation effects caused by sustained release of Mg(2+)/curcumin from injectable self-healing hydrogels, Theranostics 11 (2021) 5911–5925, https://doi.org/10.7150/thno.56266.
[19] Y. Xiong, B. Zhao, W. Zhang, L. Jia, Y. Zhang, X. Xu, Curcumin promotes osteogenic differentiation of periodontal ligament stem cells through the PI3K/AKT/Nrf2 signaling pathway, Iran J. Basic Med. Sci. 23 (2020) 954–960, https://doi.org/10.22038/IJBMS.2020.44070.10351.
[20] L. Zhu, S.J. Jia, T.J. Liu, L. Yan, D.G. Huang, Z.Y. Wang, D.J. Hao, Aligned PCL fiber conduits immobilized with nerve growth factor gradients enhance and direct sciatic nerve regeneration, Adv. Funct. Mater. 30 (2020), 2002610. ARTN_2002610_10.1002/adfm.202002610.
[21] X. Bai, M. Gao, S. Syed, J. Zhuang, X. Xu, X.Q. Zhang, Bioactive hydrogels for bone regeneration, Bioact. Mater. 3 (2018) 401–417, https://doi.org/10.1016/j.bioactmat.2018.05.006.
[22] M. Du, Q. Li, J. Chen, K. Liu, C. Song, Design and characterization of injectable abalone shell/calcium sulfate bone cement scaffold for bone defect repair, Chem. Eng. J. 420 (2021), 129866, https://doi.org/10.1016/j.cej.2021.129866.
[23] J. Zhang, X. Ma, D. Lin, H. Shi, Y. Yuan, W. Tang, C. Liu, Magnesium modification of a calcium phosphate cement alters bone marrow stromal cell behavior via an integrin-mediated mechanism, Biomaterials 53 (2015) 251–264, https://doi.org/10.1016/j.biomaterials.2015.02.097.
[24] I. Firkowska-Boden, R. Adjiski, A.C. Bautista, A. Borowski, G. Matziolis, K.D. Jandt, J. Bossert, Biopolymer surface modification of PLGA fibers enhances interfacial shear strength and supports immobilization of rhGDF-5 in fiber-reinforced brushite cement, J. Mech. Behav. Biomed. Mater. 115 (2021), 104285, https://doi.org/10.1016/j.jmbbm.2020.104285.
[25] A.R. Cho, H.K. Kim, J.Y. Kwon, T.K. Kim, Y.M. Choi, K.H. Kim, The incorporation of platelet-rich plasma into calcium phosphate cement enhances bone regeneration in osteoporosis, Pain Physician 17 (2014) E737–E745.
[26] M.H. Hu, P.Y. Lee, W.C. Chen, J.J. Hu, Incorporation of collagen in calcium phosphate cements for controlling osseointegration, Materials 10 (2017), https://doi.org/10.3390/ma10080910.
[27] M. Ventura, O.C. Boerman, G.M. Franssen, E. Bronkhorst, J.A. Jansen, X.F. Walboomers, Monitoring the biological effect of BMP-2 release on bone healing by PET/CT, J. Contr. Release 183 (2014) 138–144, https://doi.org/10.1016/j.jconrel.2014.03.044.
[28] X. Wang, Y. Yu, L. Ji, Z. Geng, J. Wang, C. Liu, Calcium phosphate-based materials regulate osteoclast-mediated osseointegration, Bioact. Mater. 6 (2021) 4517–4530, https://doi.org/10.1016/j.bioactmat.2021.05.003.
[29] K. Xiong, J. Zhang, Y. Zhu, L. Chen, J. Ye, Zinc doping induced differences in the surface composition, surface morphology and osteogenesis performance of the calcium phosphate cement hydration products, Mater. Sci. Eng. C Mater. Biol. Appl. 105 (2019), 110065, https://doi.org/10.1016/j.msec.2019.110065.
[30] S. Tan, Y. Wang, Y. Du, Y. Xiao, S. Zhang, Injectable bone cement with magnesium-containing microspheres enhances osteogenesis via anti-inflammatory immunoregulation, Bioact. Mater. 6 (2021) 3411–3423, https://doi.org/10.1016/j.bioactmat.2021.03.006.
[31] X. Cui, Y. Zhang, J. Wang, C. Huang, Y. Wang, H. Yang, H. Pan, Strontium modulates osteogenic activity of bone cement composed of bioactive borosilicate glass particles by activating Wnt/beta-catenin signaling pathway, Bioact. Mater. 5 (2020) 334–347, https://doi.org/10.1016/j.bioactmat.2020.02.016.
[32] G. Juszczyk, J. Mikulska, K. Kasperek, D. Pietrzak, W. Mrozek, M. Herbet, Chronic stress and oxidative stress as common factors of the pathogenesis of depression and alzheimer's disease: the role of antioxidants in prevention and treatment, Antioxidants 10 (2021), https://doi.org/10.3390/antiox10091439.
[33] S. Banerjee, C. Ji, J.E. Mayfield, A. Goel, J. Xiao, J.E. Dixon, X. Guo, Ancient drug curcumin impedes 26S proteasome activity by direct inhibition of dual-specificity tyrosine-regulated kinase 2, Proc. Natl. Acad. Sci. U. S. A. 115 (2018) 8155–8160, https://doi.org/10.1073/pnas.1806797115.
[34] K. Khezri, S. Maleki Dizaj, Y. Rahbar Saadat, S. Sharifi, S. Shahi, E. Ahmadian, F. Lotfipour, Osteogenic differentiation of mesenchymal stem cells via curcumin-containing nanoscaffolds, Stem Cell. Int. 2021 (2021), 1520052, https://doi.org/10.1155/2021/1520052.
[35] M. Samiei, A. Abedi, S. Sharifi, S. Maleki Dizaj, Early osteogenic differentiation stimulation of dental pulp stem cells by calcitriol and curcumin, Stem Cell. Int. 2021 (2021), 9980137, https://doi.org/10.1155/2021/9980137.
[36] Q. Yang, S.A. Leong, K.P. Chan, X.L. Yuan, T.K. Ng, Complex effect of continuous curcumin exposure on human bone marrow-derived mesenchymal stem cell regenerative properties through matrix metalloproteinase regulation, Basic Clin. Pharmacol. Toxicol. 128 (2021) 141–153, https://doi.org/10.1111/bcpt.13477.
[37] X.F. Liu, J.L. Hao, T. Xie, N.J. Mukhtar, W. Zhang, T.H. Malik, D.D. Zhou, Curcumin, A potential therapeutic candidate for anterior segment eye diseases: a review, Front. Pharmacol. 8 (2017) 66, https://doi.org/10.3389/fphar.2017.00066.
[38] J.M. Landeros, F. Belmont-Bernal, A.T. Perez-Gonzalez, M.I. Perez-Padron, P. Guevara-Salazar, I.G. Gonzalez-Herrera, P. Guadarrama, A two-step synthetic strategy to obtain a water-soluble derivative of curcumin with improved antioxidant capacity and in vitro cytotoxicity in C6 glioma cells, Mater. Sci. Eng. C Mater. Biol. Appl. 71 (2017) 351–362, https://doi.org/10.1016/j.msec.2016.10.015.
[39] Z. Chen, F. Zhang, H. Zhang, L. Cheng, K. Chen, J. Shen, W. Cui, DNA-grafted hyaluronic acid system with enhanced injectability and biostability for photo-controlled osteoarthritis gene therapy, Adv. Sci. 8 (2021), 2004793, https://doi.org/10.1002/advs.202004793.
[40] H. Yang, L. Song, B. Sun, D. Chu, L. Yang, M. Li, J. Guo, Modulation of macrophages by a paeoniflorin-loaded hyaluronic acid-based hydrogel promotes diabetic wound healing, Mater. Today Bio. 12 (2021), 100139, https://doi.org/10.1016/j.mtbio.2021.100139.
[41] W.T. Lee, J. Lee, H. Kim, N.T. Nguyen, E.S. Lee, K.T. Oh, Y.S. Youn, Photoreactive-proton-generating hyaluronidase/albumin nanoparticles-loaded PEG-hydrogel enhances antitumor efficacy and disruption of the hyaluronic acid extracellular matrix in AsPC-1 tumors, Mater. Today Bio. 12 (2021), 100164, https://doi.org/10.1016/j.mtbio.2021.100164.
[42] E. Schultze, K. Coradini, P. Dos Santos Chaves, L.P. da Silva, J. Buss, S.S. Guterres, F.K. Seixas, Drug-loaded nanoemulsion as positive control is an alternative to DMSO solutions for in vitro evaluation of curcumin delivery to MCF-7 cells, Pharmacol. Rep. 69 (2017) 1408–1412, https://doi.org/10.1016/j.pharep.2017.05.003.
[43] N. Ohbayashi, M. Shibayama, Y. Kurotaki, M. Imanishi, T. Fujimori, N. Itoh, S. Takada, FGF18 is required for normal cell proliferation and differentiation during osteogenesis and chondrogenesis, Genes Dev. 16 (2002) 870–879, https://doi.org/10.1101/gad.965702.
[44] J. Wei, X. Zhang, Z. Zhang, X. Ding, Y. Li, Y. Zhang, J. Shi, Switch-on mode of bioenergetic channels regulated by curcumin-loaded 3D composite scaffold to steer bone regeneration, Chem. Eng. J. 452 (2023), https://doi.org/10.1016/j.cej.2022.139165.
[45] A. Roy, S. Jhunjhunwala, E. Bayer, M. Fedorchak, S.R. Little, P.N. Kumta, Porous calcium phosphate-poly (lactic-co-glycolic) acid composite bone cement: a viable tunable drug delivery system, Mater. Sci. Eng. C Mater. Biol. Appl. 59 (2016) 92–101, https://doi.org/10.1016/j.msec.2015.09.081.
[46] X. Wang, J. Ye, Y. Wang, X. Wu, B. Bai, Control of crystallinity of hydrated products in a calcium phosphate bone cement, J. Biomed. Mater. Res. 81 (2007) 781–790, https://doi.org/10.1002/jbm.a.31059.
[47] H.X. Zhang, G.Y. Xiao, X. Wang, Z.G. Dong, Z.Y. Ma, L. Li, L. Nie, Biocompatibility and osteogenesis of calcium phosphate composite scaffolds containing simvastatin-loaded PLGA microspheres for bone tissue engineering, J. Biomed. Mater. Res. 103 (2015) 3250–3258, https://doi.org/10.1002/jbm.a.35463.
[48] R.P. del Real, J.G. Wolke, M. Vallet-Regi, J.A. Jansen, A new method to produce macropores in calcium phosphate cements, Biomaterials 23 (2002) 3673–3680, https://doi.org/10.1016/s0142-9612(02)00101-1.
[49] B. Cai, D. Lin, Y. Li, L. Wang, J. Xie, T. Dai, S.G.F. Shen, N2-Polarized neutrophils guide bone mesenchymal stem cell recruitment and initiate bone regeneration: a missing piece of the bone regeneration puzzle, Adv. Sci. 8 (2021), e2100584, https://doi.org/10.1002/advs.202100584.
[50] V. Kant, A. Gopal, D. Kumar, N.N. Pathak, M. Ram, B.L. Jangir, D. Kumar, Curcumin-induced angiogenesis hastens wound healing in diabetic rats, J. Surg. Res. 193 (2015) 978–988, https://doi.org/10.1016/j.jss.2014.10.019.